RSC Advances

PAPER

View Article Online
View Journal | View Issue

Cite this: *RSC Adv.*, 2020, **10**, 41720

Ionothermal synthesis of a photochromic inorganic–organic complex for colorimetric and portable UV index indication and UVB detection†

Junbiao Wu,* Luqi Lou, Yide Han, Yan Xu, Xia Zhang and Zhuopeng Wang

Received 28th September 2020
Accepted 28th October 2020

DOI: 10.1039/d0ra08300c

rsc.li/rsc-advances

Extended exposure to sunlight or artificial UV sources (particularly UVA and UVB) is a major cause of serious skin cancers and ocular diseases. A photochromic inorganic–organic complex was ionothermally synthesized *via* a decomposition-reassembly strategy, generated from a low-cost deep-eutectic solvent and a 4,4′-bipyridine system. Benefiting from the intrinsic synergy of the hydrogen bonding and π–π stacking interactions, the complex exhibited insensitivity towards visible light, outstanding color contrast from colorless to purple, rapid response time up to seconds, excellent reversibility and high thermal stability. UV index and UVB detection procedures indicated that the coloration performances of the complex exhibited a linear response towards UV index and UVB dose. Besides, the complex can be made to a portable test tablet, a freestanding mixed film with a cellulose paper and a mixed-matrix membrane with PVDF, which make it highly promising for portable and efficient visual UV index and detecting UVB dose.

Introduction

Light detection particularly in the ultraviolet (UV) spectral range has attracted significant attention over the past decades because of its wide applications in environmental safety, healthcare, industries and military.[1] Extended exposure to sunlight or artificial UV sources is a major cause of serious skin cancers and ocular diseases.[2] In particular, UVA (315–400 nm) has been shown to be involved in immunosuppression and is suspected to play a major role in melanoma induction, which is the most severe type of skin cancers.[3] UVB (280–315 nm) is implicated in the induction of cataract induction, which is the most common cause of blindness globally.[4] UVC (200–280 nm) cannot penetrate the earth's protective ozone layer to be a threat to living beings on earth. Thus, it is of great demand to explore convenient materials for the efficient detection of the UV exposure dose with specific response towards UVA and UVB, respectively.

Traditional UV photodetectors are conventionally constructed with wide-band gap semiconductors such as nitride-based,[5] silicon-based,[6] ZnO[7,8] and certain organic materials.[9] However, they suffer from poor selectivity towards visible and infrared (IR) light, limited lifetimes due to degradation under prolonged UV exposure and difficulties in fabrication,[5] which restrict their practical applications. Tremendous efforts have been devoted to achieve convenient devices with visible-blindness, rapid response time and adequate resolution and to fulfill the largely expanded needs for high-performance UV photodetectors.[10,11] To the best of our knowledge, most of the reported UV photodetectors respond to either UVA, UVC, or even wide-band UV light, and there are only a few reports on the selective UVB detection behavior.[6,8,10–12]

Recently, photochromic viologen-based metal organic frameworks (PV-MOFs) appear to offer a convenient route to monitor UV radiation.[13–15] Differently from the traditional semiconductor UV photodetectors based on the photocurrent or photovoltaic phenomenon, PV-MOFs possess excellent reversibility, fast photoresponse rates and noticeable color contrast, which makes them able to detect UV light conveniently by visual color change. Benefiting from their structural diversity and tunability, PV-MOFs may have an adequate bandgap, which makes them insensitive towards visible light and to be used as visible-blind detectors. However, the application of the PV-MOF-based detectors is still limited by some issues, particularly the difficulties in synthesis, *e.g.*, requirement of a well elaborated structural design, complicated ligand synthesis, high cost and high toxicity raw materials.[16] Therefore, it is of great significance to find a convenient and cost-effective synthetic route to construct UV light monitors based on photochromic materials. The ionothermal synthesis method has been proven to be an efficient synthetic route for exploring

Department of Chemistry, College of Sciences, Northeastern University, Shenyang, Liaoning 110819, P. R. China. E-mail: wujunbiao@mail.neu.edu.cn

† Electronic supplementary information (ESI) available: Crystal data, hydrogen bonds, additional table and figures. CCDC 1944424. For ESI and crystallographic data in CIF or other electronic format see DOI: 10.1039/d0ra08300c

novel inorganic–organic hybrid materials, such as zeolites and metal organic frameworks.[17–20] The two components, *i.e.*, ionic salts and neutral organic hydrogen-bond donors, in a low-cost deep eutectic solvent (DES), which is a kind of ionic liquid, have the potential to self-assemble or decomposition-reassemble during the ionothermal synthesis process,[21–24] implying that it is possible to find a cost-effective route to the explored new class of photochromic materials.

Herein, we present a photochromic inorganic–organic complex $|C_{10}N_2H_{10}|_2|C_{10}N_2H_8|[Ga_2(C_2O_4)_5]$ (denoted NEU20) synthesized under ionothermal conditions *via* the decomposition-reassembly strategy, generated from a low-cost deep-eutectic solvent (DES) and a 4,4′-bipyridine (bpy) system. Benefiting from the intrinsic synergy of the N–H···O hydrogen bonding and π–π stacking interactions, NEU20 exhibited insensitivity towards visible light, outstanding color contrast from colorless to purple, rapid response time up to seconds, high thermal stability and excellent reversibility. UV index and UVB detection procedures indicated that the coloration performances of the complex exhibited a linear response towards UV index and UVB dose. Besides, the complex could be made to the portable test tablet, a freestanding mixed film with a cellulose paper and a mixed-matrix membrane with PVDF, which make it highly promising for portable and efficient visual UV index and detecting UVB dose.

Experimental section

Preparation

The reagents and solvents employed were commercially available and used as received without further purification.

NEU-20. Typically, $|C_{10}N_2H_{10}|_2|C_{10}N_2H_8|[Ga_2(C_2O_4)_5]$ (denoted NEU20) was obtained from a reaction mixture of Ga_2O_3 (0.094 g, 0.5 mmol), 4,4′-bipyridine (0.156 g, 1 mmol), $H_2C_2O_4$ (1.891 g, 15 mmol) and choline chloride (0.698 g, 5 mmol) with a molar composition of 1.0 GaO : 1.0 4,4′-bipyridine : 15.0$H_2C_2O_4$: 5.0 choline chloride at 140 °C for 3 days in a Teflon-lined stainless steel autoclave under static conditions in an oven. The resulting colorless single crystals of NEU20 were collected and washed with deionized water and dried at 60 °C. Yield based on Ga was 50.1%. The H_2bpy^{2+} cations were *in situ* generated by the reaction of 4,4′-bipyridine and decomposition of the ionic portion of DES, which is less toxic and more efficient as compared to the directly used viologen derivatives. The phase purity of NEU20 was confirmed by the well agreement between the experimental PXRD pattern and the simulated one based on the structural analysis.

NEU-20 tablet. 0.1 g of the crystal material and compress with the HY-12 tablet press to obtain NEU20 tablet (diameter 1 cm).

NEU-20/PAPER. A certain amount of finely powdered NEU20 and EG (4 ml) were mixed and sonicated to form a homogenous solution. The solution was drop-casted directly on a cellulose filter paper substrate and then dried in an oven at room temperature for 12 h. The dried rewritable paper was pressed between two glass plates to form a flat rewritable paper.

NEU20/PVDF. In a typical procedure, finely powdered NEU20 particles in a definite amount were fully dispersed in DMF, to which PVDF and PVP were added in the predetermined amounts. Furthermore, the mixture was maintained at 80 °C for 8 h under continuous stirring and then aged at room temperature for about 24 h till the bubbles completely disappeared. The suspension was coated on a glass plate using a dip-coater; subsequently, the glass plate was placed in deionized water, and finally, the NEU20/PVDF mixed-matrix membrane was obtained.

Characterization

Powder X-ray diffraction (PXRD) data were collected on a PANalytical B.V. Empyrean XRD instrument with Cu-Kα radiation (λ = 1.5418 Å). *In situ* temperature dependent X-ray diffraction data were collected on a Rigaku D-Max 2550 diffractometer using Cu Kα radiation (λ = 1.5418 Å) at a heating rate of 10 °C min^{-1}. Elemental analysis was conducted on a PerkinElmer 2400 elemental analyzer (found: C 45.74%, H 2.87% and N 8.01%) (calc. C 45.66%, H 2.68% and N 7.99%). Thermogravimetric (TG) analysis was carried out on a TA Q500 analyzer in air at a heating rate of 10 °C min^{-1} from RT to 800 °C. It gave an obvious weight loss of *ca.* 81.28 wt% from 350 °C to 800 °C (Fig. S3†), corresponding to the loss of H_2bpy^{2+} cations, bpy and oxalate in one unit cell (calc. 82.19 wt%). The time-dependent UV/Vis absorption spectra were recorded at room temperature on a Lambda 650 spectrophotometer. The electron paramagnetic resonance (EPR) spectroscopy was obtained on a JEOL JES-FA200 EPR spectrometer. Fourier transform infrared (FTIR) spectra were obtained on a Bruker Equinox 55 spectrometer in the 400–4000 cm^{-1} region using a KBr disk.

Single-crystal X-ray diffraction

A suitable single crystal with dimensions of 0.20 × 0.20 × 0.20 mm^3 for NEU20 was selected for the single-crystal X-ray diffraction analysis. The intensity data were collected on a CrystalClear-SM Expert 2.0 r1 (Rigaku, 2009) CCD diffractometer by oscillation scans using the graphite-monochromated Mo Kα radiation (λ = 0.71073 Å) at 23 ± 2 °C. Cell refinement and data reduction were accomplished with the SAINT processing program.[25] The structure was solved in a monoclinic space group *C*2/*c* (No. 15) by the direct methods and refined by the full matrix least-squares technique with the SHELXTL crystallographic software package.[26] All framework atoms Ga, C, N and O could be unambiguously located. All non-hydrogen atoms were refined anisotropically. The hydrogen atoms were calculated in ideal positions and were refined by riding on their respective nitrogen atoms. Experimental details for the structure determination are presented in Table S1.†

UV index (UVI) and UV dose detection procedures

For the UVI-dependent coloration measurements, a 300 W xenon lamp (PLS-SEX300/300 UV type, CEAULIGHT Beijing) was used as the irradiation source. The UV light intensity was measured by a PM100D photometer (Thorlabs GmbH). The UVI

value obtained from the lamp was measured with a PM100D photometer (Thorlabs GmbH) and controlled with the distance between the lamp and the NEU20 tablet sample. For UVA and UVB coloration, the irradiation setup was the same as described for UVI detection, except for the irradiation sources were UV lamps (365 nm-UVA and 311 nm-UVB Philips). An exposure time of 120 s was used to ensure reaching color saturation. Under environmental conditions, the samples were exposed to a UV light for 2 min, and then the discolored sample was obtained (the light intensity values were 5, 10, 15, 30, 45 W m^{-2}, the corresponding UV indices were 2, 4, 6, 8, 10 and the UV doses were 60, 120, 180, 360, 540 mJ cm^{-2}). The color detection was taken with a common smart phone, and then converted the *RGB* value of the photos to grayscale calculating the ratio of the grayscale of the unirradiated sample and the tested samples. I = rgb2gray (*RGB*) converted the true color image *RGB* to the grayscale intensity image I. rgb2gray converted *RGB* values to grayscale values by forming a weighted sum of the R, G, and B components: $0.2989 \times R + 0.5870 \times G + 0.1140 \times B$.[27]

Results and discussion

Crystal structure

Colorless NEU20 crystallized in the monoclinic space group $C2/c$ (No. 15). The X-ray single-crystal structural analysis indicated that NEU20 was constructed with anionic $Ga_2(C_2O_4)_5^{4-}$ clusters, and templated by one neutral bpy and two diprotonated bpy cations (H_2bpy^{2+}), which compensated the negative charges (Fig. 1a). The unique Ga site was hexa-coordinated with three bidentate carboxylate groups of the oxalate, and the two Ga^{3+} ions were linked by sharing the oxalate to form an anionic $Ga_2(C_2O_4)_5^{4-}$ cluster. The Ga–O bond distances varied from 1.939(5) Å to 2.076(6) Å. There were strong N–H···O hydrogen bonding interactions between the oxygen atoms of oxalate and H_2bpy^{2+} with D···A separations [d(D···A)] varying from 2.834(10) Å to 2.880(9) Å (Fig. 1b), and weak N–H···O hydrogen interactions between the oxygen atoms of oxalate and the bpy/H_2bpy^{2+} with D···A separations [d(D···A)] varying from 3.096(10) Å to 3.503(11) Å (Table S2†). The N–H···O hydrogen bonds were weaker than that of other bpy and carboxylic acid-related photochromic MOFs ([d(D···A)] 2.521(1) Å to 2.660(6) Å), and maybe the potential paths for the through-space electron transfer.[28–30] In addition, π–π stacking interactions were found between the adjacent pyridinium rings of the bpy and H_2bpy^{2+} dications with face-to-face distances from 3.514(108) Å to 3.730(87) Å (Fig. 1b).

Photochromism

NEU20 is photoactive and exhibits a rapid naked eye-detectable colour change from colorless to purple in seconds upon UV light irradiation (30 W, 365 nm) under ambient conditions. *In situ* time dependent UV/Vis spectra emerged three new adsorption bands at 387 nm, 556 nm and 599 nm upon 3 s UV irradiation (Fig. 2a), and the intensity of these peaks increased with prolonged irradiation time accompanied by the gradual color change of irradiated samples (denoted NEU20-P) from colorless to deeper purple. The observed peaks are similar to the characteristic absorption of one-electron reduced species of viologen compounds *via* photoinduced electron transfer (PIET).[16,28] *In situ* time dependent UV-Vis spectra monitored at 599 nm indicated that the PIET process followed a first order reaction kinetics, with a rate constant k_{obs} of 0.195 s^{-1}, which was much higher than that of some reported viologen-based photochromic compounds (2.324×10^{-4} s^{-1} to 1.5×10^{-2} s^{-1}),[31,32] indicating its superior

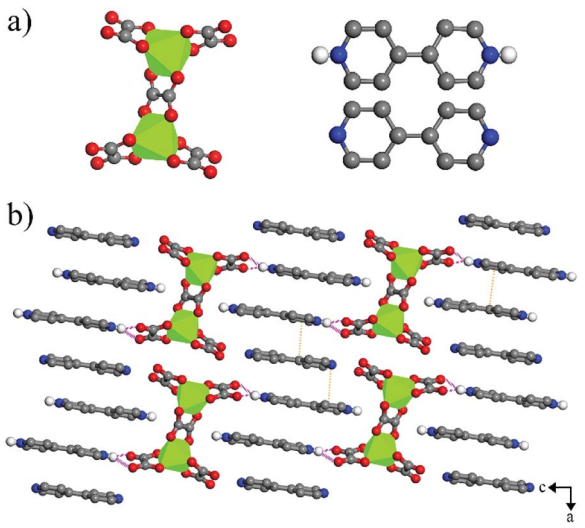

Fig. 1 (a) Building units of NEU20; (b) N–H···O H-bonding interactions between the oxygen atoms of oxalate and H_2bpy^{2+} (purple dotted line) and face-to-face π–π stacking interactions between the adjacent pyridinium rings of the bpy and H_2bpy^{2+} dications (yellow dotted line) along the [010] direction. Color: O, red; C, gray; H, white; N, blue; Ga, green.

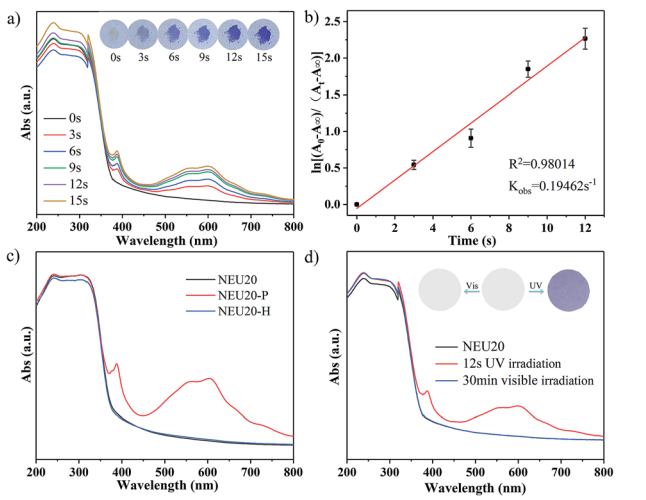

Fig. 2 (a) *In situ* time dependent UV-Vis spectra of NEU20 by UV light irradiation; (b) first-order kinetic plot for change in absorbance with error bars at λ = 599 nm, where A_0, A_t, and A_∞ are the absorbance values at time zero, time t, and infinite time of the reaction, respectively; (c) UV-Vis spectra of NEU20, NEU20-P and NEU20-H; (d) UV-Vis spectra and photos of NEU20 and after 12 s UV irradiation, after 30 min visible irradiation, respectively.

photoresponsive rate (Table S3†). NEU20-P could be retained under ambient conditions for several months with no naked eye-detectable color change, indicating an ultralong-lived charge-separated state and excellent colored stability upon UV irradiation, which may be attributed to the π–π stacking interactions and the dense packing mode of bpy/H_2bpy^{2+} dications that stabilized the generated radicals and prevented the electron transfer between the radicals and inorganic clusters.[33–35] NEU20-P could be completely decoloured through annealing at 140 °C for 10 min or 80 °C for 2 h in air, indicating that the coloration–decoloration process of NEU20 was reversible. This reversible photochromic transformation could be repeated several cycles by alternatively treating with UV irradiation and heating without noticeable change in the photochromic properties.

To further confirm the PIET process during photochromic transformation, electron paramagnetic resonance (EPR) and X-ray photoelectron spectroscopy (XPS) measurements were performed. EPR spectra indicate that no EPR signal is detected from the original NEU20 but a single-line signal closed to that of a free electron at $g = 2.0048$ is observed after irradiation, and it disappeared after thermally bleached (Fig. 3a). DFT calculations indicate that electrons on the oxalate were unfavorable to migrate to bpy, but electron transfer between the H_2bpy^{2+} and oxalate could be realized,[28] so the paramagnetic center of NEU20-P should be the $H_2bpy^{\bullet+}$ radicals. The variation of O 1s and N 1s in the XPS spectra before and after the irradiation also gave insights into the PIET process (Fig. 3b and c). Electron dissociation from the oxygen atoms resulted in a shift to a higher binding energy in the O 1s core-level spectra. As for the N 1s core-level spectra, the peaks at 398.0 eV assigned to the free nitrogen in bpy were similar, while the peaks at 401.5 eV attributed to the protonated N in H_2bpy^{2+} notably shifted to a lower N 1s binding energy, indicating H_2bpy^{2+} received the electrons. All these results confirmed that H_2bpy^{2+} ions were reduced to $H_2bpy^{\bullet+}$ radicals after irradiation, and the $H_2bpy^{\bullet+}$ radicals recovered to H_2bpy^{2+} upon heating during the coloration–decoloration processes. The PIET process under nitrogen atmosphere exhibited that NEU20 underwent a rapid visible photochromic transformation from colorless to purple upon UV light irradiation, the sample color changed from purple to colorless after heating at 140 °C for 10 min, which indicated that the bleach process was just thermal quenching and not an oxygen-mediated process.

Stability

High thermal stability is vital for the practical applications of photochromic materials processed in various forms. The thermal stability of NEU20 was confirmed by *in situ* temperature dependent XRD (Fig. S2†) and TG analyses (Fig. S3†). By comparing the PXRD patterns obtained at different temperatures, it was found that the structure remained intact until 350 °C, and no thermochromic behavior was found in this process. UV/Vis spectra (Fig. 2c), XRD patterns (Fig. S4†) and IR spectra (Fig. S5†) show consistent results that the structure of NEU20 is stable during the reversible photochromic transformation.

UVI and UV dose detection

It is worth noting that the photochromic behavior was not be observed under visible light illumination (300 W xenon lamp with 420 nm cut-off filter), and no clear change was observed in the UV-Vis spectra (Fig. 2d), which may be attributed to the longer charge transfer pathway, thus ensuring that NEU20 can be used as a visible-blind sensor. In addition, a relatively large optical energy gap (E_g) (3.40 eV) of NEU20 was obtained *via* the calculation based on the diffuse reflectance spectrum (Fig. S6†), which further supported its potential for UV light photodetectors.

With regards to its insensitivity towards visible light, outstanding color contrast from colorless to purple, superior photoresponsive rate, high thermal stability and easy recovery under heating, NEU20 was made into tablets (diameter 1 cm) for UV index (UVI) and UV dose detection. The coloration performances of NEU20 were performed under a xenon lamp and UV lamps (365 nm-UVA and 311 nm-UVB) using a 120 s exposure time (to ensure reaching the color saturation) at different UVI values and UV doses. Different from the reported PV-MOF UV detectors recording absorbance, as characterized by a spectrophotometer, a simple procedure was established for the color detection, in which photos of the unirradiated sample and the tested samples were first taken with a common smart phone, followed by calculating grayscale ratios after the photos

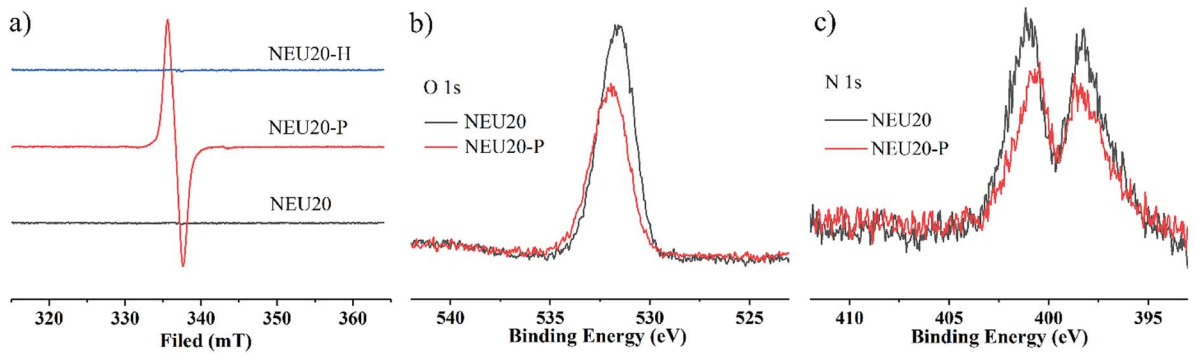

Fig. 3 (a) EPR spectra of NEU20, NEU20-P and NEU20-H; (b) O 1s XPS core-level spectra of NEU20 and NEU20-P; (c) N 1s XPS core-level spectra of NEU20 and NEU20-P.

were converted into grayscale images. The color change is illustrated in Fig. 4a, indicating that NEU20 exhibited a good response towards UVI values and there is a linear relationship between the grayscale ratios and the UV index. Moreover, clear coloring could be achieved below UVI 4, upon which protective measures should be taken to avoid sunburn. This suggested that NEU20 could be used as an efficient UVI indicator, and it would be suitable for UVI quantification. The levels of UVA and UVB components were detectable using a procedure similar to that described above based on the observed different color change deviation (Fig. 4b and S7†). As shown in Fig. 4b, the results showed a clearly detectable dependence between the grayscale ratios and the UVB doses, which followed a first order reaction kinetics, suggesting a high potential for use in UVB dosimetry.

Machinability

It is very important but also challenging to manufacture the photochromic materials into forms that can be used in actual devices. The development of films based on these materials is still in its nascent stages. Besides tablets, NEU20 was also made into freestanding mixed films with a cellulose filter paper (NEU20 PAPER) though the drop-casting method and mixed-matrix membranes with PVDF (NEU20/PVDF) though the lyophase conversion process to investigate its machinability (Fig. 5a). As an example, we demonstrated the excellent color contrast of NEU20 PAPER before and after the UV irradiation, and the good recovery property by alternating treatments with

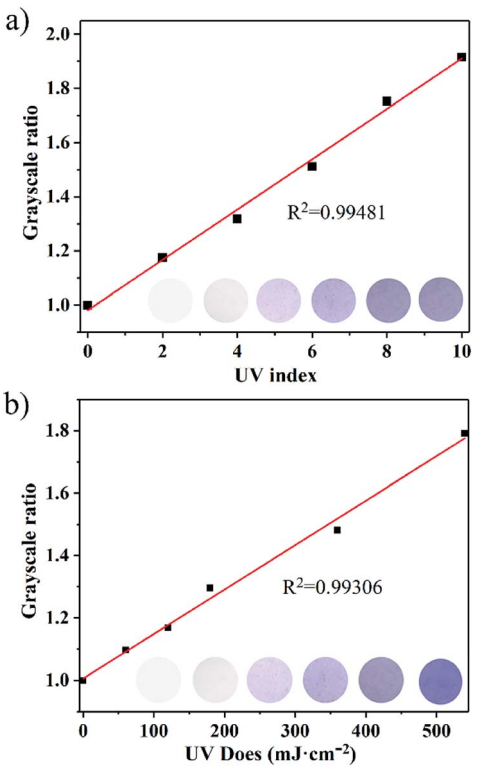

Fig. 4 (a) Color intensity of NEU20 at different UV index values; (b) UVB doses detected with NEU20. The grayscale ratios were obtained from the photos shown in the insets.

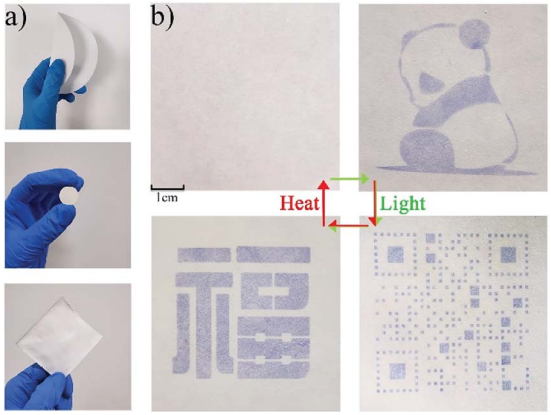

Fig. 5 (a) Photographs of the NEU20 PAPER (top), NEU20 tablet (middle) and NEU20/PVDF (bottom); (b) photograph of the contents printed on the NEU20 PAPER and 4 coloration–decoloration rounds with alternating UV irradiation for 2 min and heating under 80 °C for 2 h.

UV irradiation and heating (Fig. 5b). In addition, the colored state of NEU20 PAPER and NEU20/PVDF could be retained under ambient conditions for 90 days, which were much more stable than other reported photochromic papers (Fig. S8†).[36–40] The diverse machinability indicated that NEU20 could be used as a portable UV detector and could be applied as an inkless and erasable printing medium.

Conclusions

In conclusion, a photochromic inorganic–organic complex was ionothermally synthesized *via* a decomposition-reassembly strategy in a low-cost DES and a bpy system. Benefiting from the intrinsic synergy of the N–H···O hydrogen bonding and π–π stacking interactions, NEU20 featured insensitivity towards visible light, outstanding color contrast from colorless to purple, rapid response time up to seconds, excellent reversibility and high thermal stability. UV index and UVB detection procedures indicated that the coloration performances of the complex exhibited a linear response towards the UV index and UVB dose. Besides, the complex could be made into the portable test tablet, a freestanding mixed film with a cellulose paper and a mixed-matrix membrane with PVDF, which make it highly promising for colorimetric and portable UV index indication and UVB dose detection. This work provides a low-cost route to synthesize photochromic materials and sheds a light on the design of portable visual UV detectors in healthcare.

Conflicts of interest

There are no conflicts of interest to declare.

Acknowledgements

This work was financially supported by the National Natural Science Foundation of China (No. 21601029, 21601030), and the Fundamental Research Funds for the Central Universities of China (No. N2005021).

Notes and references

1 D. Gedamu, I. Paulowicz, S. Kaps, O. Lupan, S. Wille, G. Haidarschin, Y. K. Mishra and R. Adelung, Rapid fabrication technique for interpenetrated ZnO nanotetrapod networks for fast UV sensors, *Adv. Mater.*, 2014, **26**, 1541–1550.

2 P. Gies, E. van Deventer, A. C. Green, C. Sinclair and R. Tinker, Review of the global solar UV index 2015 workshop report, *Health Phys.*, 2018, **114**, 84–90.

3 S. Mouret, C. Baudouin, M. Charveron, A. Favier, J. Cadet and T. Douki, Cyclobutane pyrimidine dimers are predominant DNA lesions in whole human skin exposed to UVA radiation, *Proc. Natl. Acad. Sci. U. S. A.*, 2006, **103**, 13765–13770.

4 H. R. Taylor and C. A. McCarty, A review of the epidemiologic evidence linking ultraviolet radiation and cataracts, *Dev. Ophthalmol.*, 2002, **35**, 21–31.

5 E. Cicek, R. McClintock, Z. Vashaei, Y. Zhang, S. Gautier, C. Y. Cho and M. Razeghi, Crack-free AlGaN for solar-blind focal plane arrays through reduced area epitaxy, *Appl. Phys. Lett.*, 2013, **102**, 051102.

6 X. Sheng, C. Yu, V. Malyarchuk, Y. H. Lee, S. Kim, T. Kim, L. Shen, C. Horng, J. Lutz, N. C. Giebink, J. Park and J. A. Rogers, Silicon-based visible-blind ultraviolet detection and imaging using down-shifting luminophores, *Adv. Opt. Mater.*, 2014, **2**, 314–319.

7 Y. Liu, C. R. Gorla, S. Liang, H. Shen and M. Wraback, Ultraviolet detectors based on epitaxial ZnO films grown by MOCVD, *J. Electron. Mater.*, 2000, **29**, 69–74.

8 W. Yang, S. S. Hullavarad, B. Nagaraj, I. Takeuchi, R. P. Sharma, T. Venkatesan, R. D. Vispute and H. Shen, Compositionally-tuned epitaxial cubic $Mg_xZn_{1-x}O$ on Si(100) for deep ultraviolet photodetectors, *Appl. Phys. Lett.*, 2003, **82**, 3424–3426.

9 D. Ray and K. L. Narasimhan, High response organic visible-blind ultraviolet detector, *Appl. Phys. Lett.*, 2007, **91**, 093516.

10 Y. Q. Bie, Z. M. Liao, H. Z. Zhang, G. R. Li, Y. Ye, Y. B. Zhou, J. Xu, Z. X. Qin, L. Dai and D. P. Yu, Self-Powered, Ultrafast, Visible-Blind UV detection and optical logical operation based on ZnO/GaN nanoscale p–n Junctions, *Adv. Mater.*, 2011, **23**, 649–653.

11 M. Gong, Q. Liu, B. Cook, B. Kattel, T. Wang, W. L. Chan, D. Ewing, M. Casper, A. Stramel and J. Z. Wu, All-printable ZnO quantum dots/graphene van der waals heterostructures for ultrasensitive detection of ultraviolet light, *ACS Nano*, 2017, **11**, 4114–4123.

12 I. Norrbo, A. Curutchet, A. Kuusisto, J. Mäkelä, P. Laukkanen, P. Paturi, T. Laihinen, J. Sinkkonen, E. Wetterskog, F. Mamedov, T. Le Bahers and M. Lastusaari, Solar UV index and UV dose determination with photochromic hackmanites: from the assessment of the fundamental properties to the device, *Mater. Horiz.*, 2018, **5**, 569–576.

13 S. Hu, J. Zhang, S. Chen, J. Dai and Z. Fu, Efficient ultraviolet light detector based on a crystalline viologen-based metal–organic framework with rapid visible color change under irradiation, *ACS Appl. Mater. Interfaces*, 2017, **9**, 39926–39929.

14 L. Li, Z. M. Tu, Y. Hua, X. N. Li, H. Y. Wang and H. Zhang, A novel multifunction photochromic metal–organic framework for rapid ultraviolet light detection, amine-selective sensing and inkless and erasable prints, *Inorg. Chem. Front.*, 2019, **6**, 3077–3082.

15 L. Li, Y. C. Zou, Y. Hua, X. N. Li, Z. H. Wang and H. Zhang, Polyoxometalate–viologen photochromic hybrids for rapid solar ultraviolet light detection, photoluminescence-based UV probing and inkless and erasable printing, *Dalton Trans.*, 2020, **49**, 89–94.

16 J. Wu, L. Lou, H. Sun, C. Tao, T. Li, Z. Wang, X. Zhang and J. Li, Photochromic inorganic–organic complex derived from low-cost deep eutectic solvents with tunable photocurrent responses and photocatalytic properties, *CrystEngComm*, 2020, **22**, 1078–1085.

17 E. R. Cooper, C. D. Andrews, P. S. Wheatley, P. B. Webb and R. E. Morris, Ionic liquids and eutectic mixtures as solvent and template in synthesis of zeolite analogues, *Nature*, 2004, **430**, 1012–1016.

18 R. E. Morris and E. R. Parnham, Ionothermal synthesis of zeolites, metal–organic frameworks, and inorganic–organic hybrids, *Acc. Chem. Res.*, 2007, **40**, 1005–1013.

19 G. Férey, Hybrid porous solids: past, present, future, *Chem. Soc. Rev.*, 2008, **37**, 191–214.

20 H. Xing, W. Yang, T. Su, Y. Li, J. Xu, T. Nakano, J. Yu and R. Xu, Ionothermal synthesis of extra-large-pore open-framework nickel phosphite $5H_3O$ $[Ni_8(HPO_3)_9Cl_3]1.5$ H_2O: magnetic anisotropy of the antiferromagnetism, *Angew. Chem., Int. Ed.*, 2010, **49**, 2328–2331.

21 P. C. Jhang, N. T. Chuang and S. L. Wang, Layered zinc phosphates with photoluminescence and photochromism: chemistry in deep eutectic solvents, *Angew. Chem., Int. Ed.*, 2010, **49**, 4200–4204.

22 P. C. Jhang, Y. C. Yang, Y. C. Lai, W. R. Liu and S. L. Wang, A fully integrated nanotubular yellow-green phosphor from an environmentally friendly eutectic solvent, *Angew. Chem., Int. Ed.*, 2009, **48**, 742–745.

23 Q. Zhang, K. De Oliveira Vigier, S. Royer and F. Jérôme, Deep eutectic solvents: syntheses, properties and applications, *Chem. Soc. Rev.*, 2012, **41**, 7108–7146.

24 D. Carriazo, M. C. Serrano, M. C. Gutiérrez, M. L. Ferrer and F. del Monte, Deep-eutectic solvents playing multiple roles in the synthesis of polymers and related materials, *Chem. Soc. Rev.*, 2012, **41**, 4996–5014.

25 *SAINT*, Bruker AXS Inc, 5465 EastCheryl Parkway, Madison, WI, USA, 2000, pp. 53711–55373.

26 G. M. Sheldrick, Crystal structure refinement with SHELXL, *Acta Crystallogr., Sect. A: Found. Adv.*, 2015, **71**, 3–8.

27 K. Kalaivani, R. Praveena, V. Anjalipriya and R. Srimeena, Real time implementation of image recognition and text to speech conversion, *International Journal of Advanced Engineering Research and Technology*, 2014, **2**, 2348–8190.

28 Z. W. Chen, G. Lu, P. X. Li, R. G. Lin, L. Z. Cai, M. S. Wang and G. C. Guo, Influence of supramolecular interactions

on electron-transfer photochromism of the crystalline adducts of 4,4′-bipyridine and carboxylic acids, *Cryst. Growth Des.*, 2014, **14**, 2527–2531.

29 N. J. Turro and G. J. Kavarnos, Photosensitization by reversible electron transfer: theories, experimental evidence, and examples, *Chem. Rev.*, 1986, **86**, 401–449.

30 M. R. Wasielewski, Photoinduced electron transfer in supramolecular systems for artificial photosynthesis, *Chem. Rev.*, 1992, **92**, 435–461.

31 C. Sun, G. Xu, X. M. Jiang, G. E. Wang, P. Y. Guo, M. S. Wang and G. C. Guo, Design strategy for improving optical and electrical properties and stability of lead-halide semiconductors, *J. Am. Chem. Soc.*, 2018, **140**, 2805–2811.

32 S. L. Li, M. Han, Y. Zhang, G. P. Li, M. Li, G. He and X. M. Zhang, X-ray and UV dual photochromism, thermochromism, electrochromism, and amine-selective chemochromism in an anderson-like Zn_7 cluster-based 7-fold interpenetrated framework, *J. Am. Chem. Soc.*, 2019, **141**, 12663–12672.

33 R. G. Lin, G. Xu, M. S. Wang, G. Lu, P. X. Li and G. C. Guo, Improved photochromic properties on viologen-based inorganic–organic hybrids by using π-conjugated substituents as electron donors and stabilizers, *Inorg. Chem.*, 2013, **52**, 1199–1205.

34 Y. Apeloig, D. B. Zhivotovskii, V. Shklover and Y. Struchkov, Synthesis and X-ray molecular structure of the first stable organic radical lacking resonance stabilization, *J. Am. Chem. Soc.*, 1999, **121**, 8118–8119.

35 B. T. King, B. C. Noll, A. J. McKinley and J. Michl, Dodecamethylcarba-*closo*-dodecaboranyl ($CB_{11}Me_{12}$), a stable free radical, *J. Am. Chem. Soc.*, 1996, **118**, 10902–10903.

36 B. Garai, A. Mallick and R. Banerjee, Photochromic metal–organic frameworks for inkless and erasable printing, *Chem. Sci.*, 2016, **7**, 2195–2200.

37 J. Wei, X. Jiao, T. Wang and D. Chen, Electrospun photochromic hybrid membranes for flexible rewritable media, *ACS Appl. Mater. Interfaces*, 2016, **8**, 29713–29720.

38 W. Q. Kan, S. Z. Wen, Y. C. He and C. Y. Xu, Viologen-based photochromic coordination polymers for inkless and erasable prints, *Inorg. Chem.*, 2017, **56**, 14926–14935.

39 W. Wang, J. Feng, Y. Ye, F. Lyu, Y. S. Liu, J. Guo and Y. Yin, Photocatalytic color switching of transition metal hexacyanometalate nanoparticles for high-performance light-printable rewritable paper, *Nano Lett.*, 2017, **17**, 755–761.

40 Q. Shi, S. Y. Wu, X. T. Qiu, Y. Q. Sun and S. T. Zheng, Three viologen-derived Zn–organic materials: photochromism, photomodulated fluorescence, and inkless and erasable prints, *Dalton Trans.*, 2019, **48**, 954–963.